



Published in final edited form as:

Science. 2007 November 9; 318(5852): 980–985. doi:10.1126/science.1147851.

Magnetic Resonance Spectroscopy Identifies Neural Progenitor Cells in the Live Human Brain

Louis N. Manganas^{1,3}, Xueying Zhang¹, Yao Li¹, Raphael D. Hazel^{1,2}, S. David Smith², Mark E. Wagshul¹, Fritz Henn², Helene Benveniste^{1,2}, Petar M. Djuri¹, Grigori Enikolopov^{3,*}, and Mirjana Maletić-Savati^{1,3,*}

¹SUNY Stony Brook, Stony Brook, NY 11794, USA

²Brookhaven National Laboratory, Upton, NY 11719, USA

³Cold Spring Harbor Laboratory, Cold Spring Harbor, NY 11724, USA

Abstract

The identification of neural stem and progenitor cells (NPCs) by in vivo brain imaging could have important implications for diagnostic, prognostic, and therapeutic purposes. We describe a metabolic biomarker for the detection and quantification of NPCs in the human brain in vivo. We used proton nuclear magnetic resonance spectroscopy to identify and characterize a biomarker in which NPCs are enriched and demonstrated its use as a reference for monitoring neurogenesis. To detect low concentrations of NPCs in vivo, we developed a signal processing method that enabled the use of magnetic resonance spectroscopy for the analysis of the NPC biomarker in both the rodent brain and the hippocampus of live humans. Our findings thus open the possibility of investigating the role of NPCs and neurogenesis in a wide variety of human brain disorders.

The adult mammalian brain retains the ability to generate new neurons. These neurons are produced from neural stem and progenitor cells (NPCs), which reside in the hippocampus and the subventricular zone (1–4). NPCs possess the ability to self-renew and also to generate progeny that can give rise to mature cell types. The ability of NPCs to produce neurons, astrocytes, and oligodendrocytes in vitro and in vivo raises the prospect of harnessing them to repair nerve tissue damaged or lost to neurological disease or trauma (1, 2, 4). The realization of the curative potential of NPCs would benefit from the development of methods that would enable their identification and tracking in vivo. Currently, positron emission tomography, single-photon computed tomography scanning, and magnetic resonance imaging (MRI) are being examined toward this goal (5–7). These technologies require NPCs to be preloaded ex vivo with radiolabeled agents or superparamagnetic iron oxide–based derivatives, and therefore are not applied for the detection of endogenous NPCs

*To whom correspondence should be addressed. enikolop@cshl.edu (G.E.); mmaleticsava@notes.cc.sunysb.edu (M.M.-S.).

Supporting Online Material

www.sciencemag.org/cgi/content/full/318/5852/980/DC1

Materials and Methods

SOM Text

Figs. S1 to S3

in the human brain. We used proton magnetic resonance spectroscopy ($^1\text{H-MRS}$) to overcome the above limitations and to detect NPCs in the live human brain.

Proton nuclear magnetic resonance spectroscopy ($^1\text{H-NMR}$) has been widely used for in vitro detection of low quantities of known metabolites and the identification of unknown compounds present in body fluids or tissues in vitro (8). $^1\text{H-NMR}$ can identify metabolites that are specific for neurons [such as *N*-acetyl aspartate (NAA)] or glia [such as choline (Cho) and myoinositol (mI)], and these compounds have been used as reliable biomarkers of the corresponding cell types in isolated tissue samples. However, $^1\text{H-NMR}$ cannot be used to analyze metabolites in live organisms; instead, its correlate, $^1\text{H-MRS}$, is used to provide information about the metabolic status of a tissue in vivo (9). These two techniques complement each other when physiological or pathological states are investigated (10–12). Thus, we decided to search for NPC-specific metabolites using $^1\text{H-NMR}$ and then to exploit the information about these metabolites for detecting NPCs in the live brain using $^1\text{H-MRS}$.

To identify unique features in the spectroscopic profile of NPCs, we compared the $^1\text{H-NMR}$ spectra of NPCs from embryonic mouse brain tissue cultivated as neurospheres in vitro (13) with the spectra of cultured neurons, astrocytes, and oligodendrocytes (Fig. 1A). The NPC spectra demonstrated a unique profile, including a prominent peak at the frequency of 1.28 parts per million (ppm), which was not observed in other neural cell types (Fig. 1A). Quantification of the selected signal amplitude confirmed that NPCs were strongly enriched in the 1.28-ppm biomarker as compared to other cell types, whereas, as expected, NAA (2.02 ppm) was predominant in neurons and Cho (3.22 ppm) in astrocytes (Fig. 1B). Small amounts of NAA and Cho were also observed in NPCs, most likely reflecting the presence of neuron- and astrocyte-committed progenitors in the neurospheres. The 1.28-ppm biomarker was detected, to a lesser degree, in our oligodendrocyte preparation, perhaps due to the presence of oligodendrocyte progenitor cells (OPCs; also see Fig. 1D) within the primary cultures analyzed. The amplitude of the 1.28-ppm signal on the $^1\text{H-NMR}$ spectra was proportional to the number of NPCs taken for analysis (Fig. 1C); this linear correlation indicated that it is possible to quantitatively account for NPCs based on the amount of the 1.28-ppm $^1\text{H-NMR}$ signal.

To further examine the specificity of the 1.28-ppm biomarker, we compared the $^1\text{H-NMR}$ spectroscopic profile of NPCs with the profiles of embryonic stem cells (ESCs), cells of the hair follicle-derived sphere cultures (SPCs) (14), OPCs, and other types of cells that may be present in the brain, such as macrophages, T lymphocytes, and microglia. The 1.28-ppm biomarker was detected in ESCs, SPCs, and OPCs at significantly lower levels than in the NPCs and was near or below the detection limit in the resting macrophages, T lymphocytes, and microglia (Fig. 1D). We also performed experiments with cultured neurospheres derived from brains of transgenic mice expressing green fluorescent protein (GFP) under the control of nestin gene regulatory elements (13). Nestin-GFP neuro-spheres were dissociated and cells were sorted on the basis of GFP expression levels by means of fluorescence-activated cell sorting (fig. S2). NPC-enriched GFP-expressing cell populations contained higher levels of the 1.28-ppm biomarker than did GFP-negative cells (fig. S2). Together, these experiments indicate that progenitor cells of different origin (but each with neural potential) express the 1.28-ppm biomarker; that among the panel of tested cells, NPCs have the highest

level of the biomarker; and that neither postmitotic differentiated cells nor cells without progenitor properties express the biomarker.

If the presence of the 1.28-ppm biomarker correlates with the progenitor status of cells, the levels of this biomarker should decrease as cells differentiate in vitro or in vivo, whereas the levels of the biomarkers of differentiated cells should increase. We cultivated neurospheres under conditions that promote their neuronal and astrocytic differentiation and analyzed their $^1\text{H-NMR}$ spectra. The levels of the 1.28-ppm biomarker decreased, whereas the levels of the neuronal biomarker NAA and astrocytic biomarker Cho increased after several days of cultivation (Fig. 2A). We next compared the spectra of cells isolated from the mouse brain at embryonic day 12 (E12), when neurogenesis begins, and at postnatal day 30 (P30), when most of the cells in the brain have already differentiated. The levels of the 1.28-ppm biomarker were significantly reduced, whereas the levels of biomarkers of differentiated cells were significantly elevated, in the postnatal adult brain as compared to the embryonic brain (Fig. 2B).

We next examined whether neurogenic regions of the adult brain are enriched in the 1.28-ppm biomarker. We compared the $^1\text{H-NMR}$ spectra of cells isolated from the adult mouse hippocampus, where continuous neurogenesis takes place, and from the cortex, where neurogenesis is not detected (1, 2, 15). A significantly higher amount of the 1.28-ppm biomarker was observed in the adult hippocampus as compared to the cortex (Fig. 2C), providing additional evidence that the presence of the 1.28-ppm biomarker correlates with the presence of NPCs. We then analyzed whether changes in the levels of the 1.28-ppm biomarker correlate with dynamic changes in adult neurogenesis. Neurogenesis in the adult mammalian hippocampus is sensitive to a wide range of stimuli, including electroconvulsive shock (ECS) (16–21). We applied ECS to adult mice and assessed cell proliferation using bromodeoxyuridine (BrdU) incorporation in the subgranular zone of the dentate gyrus and measured levels of the 1.28-ppm biomarker using $^1\text{H-NMR}$. The number of BrdU-immunoreactive cells was significantly increased in ECS-treated, as compared to control sham-operated, animals, demonstrating the effectiveness of the procedure (Fig. 2D). The levels of the 1.28-ppm biomarker in the preparation of cells from the hippocampus were also significantly increased after ECS (Fig. 2D). Together, our results with the cultured NPCs and with the developing and adult animal brain demonstrate that the amount of 1.28-ppm biomarker correlates with neurogenesis and suggest that changes in neurogenesis can be analyzed using the 1.28-ppm biomarker as a valid reference for NPCs.

We next sought to characterize the chemical nature of the 1.28-ppm biomarker. A specific group of resonances in the 0 to 2 ppm range of the $^1\text{H-NMR}$ is thought to arise from macromolecules and the fatty acyl chains of triacylglycerides and cholesterol esters found in free-floating mobile lipids in the cytoplasm and in unrestricted lipid microdomains near the plasma membrane (22). Proton chemical shift correlation spectroscopy of NPCs showed that there was a *J*-coupling partner for the 1.28-ppm biomarker at 0.8 ppm, as would be expected for a fatty acid containing methyl ($-\text{CH}_3$) groups on the same molecule (fig. S3 and Fig. 1A). The notion that the 1.28-ppm biomarker corresponds to lipids was also supported by a decrease in the 1.28-ppm signal amplitude when neurospheres were treated with cerulenin, an inhibitor of fatty acid synthesis (Fig. 2E). To further examine whether the 1.28-ppm

biomarker contains lipids, we analyzed the ^1H -NMR spectra of NPCs extracted with a chloroform/methanol mixture. The 1.28-ppm biomarker was mainly present in the chloroform fraction, which is suggestive of a lipid metabolite (Fig. 2G). Indeed, it overlapped with some of the specific fatty acid spectra, most closely with the spectra of saturated fatty acids (SFAs), such as palmitic acid, and of monounsaturated fatty acids (MUFAs), such as oleic acid (Fig. 2G). The spectra of polyunsaturated fatty acids (PUFAs), such as arachidonic acid, which resonate in the 1.3- to 1.4-ppm range, did not overlap (Fig. 2G). Using gas chromatography, we sought to separate and quantify specific fatty acids in NPCs and compare them to those found in astrocytes. There was a higher concentration of SFAs and MUFAs than of PUFAs in NPCs, but not in astrocytes (Fig. 2F). Together, our results suggest that the 1.28-ppm biomarker is most likely a mixture of lipids that include SFAs and/or MUFAs.

We next addressed the possibility of using the NPC biomarker for in vivo brain imaging. Using a 9.4-T micro MRI (mMRI) scanner, we obtained adult rat spectra of the hippocampus, where endogenous NPCs reside, and the parietal cortex, where dividing NPCs are undetectable (Fig. 3). Traditional Fourier transform signal processing was unable to distinguish the 1.28-ppm biomarker in the hippocampus from background noise (Fig. 3A, insets), most likely due to a low NPC density in the adult rat hippocampus. Therefore, we developed a more sensitive signal-processing algorithm in order to isolate the signal of the 1.28-ppm biomarker from the noise within the in vivo ^1H -MRS spectra. We used singular value decomposition (SVD), which permits improved detection at low signal-to-noise ratios and allows better resolution of signal components (modes) that are close to one another in a given frequency domain (23–25). Based on SVD signal processing, we developed an algorithm that enables detection of the 1.28-ppm biomarker in the adult rat hippocampus in vivo (Fig. 3A, red peak). Absolute quantification of the 1.28-ppm biomarker was achieved by estimating the amplitude of the 1.28-ppm signal, whereas relative quantification was achieved by ratiometric analysis with the creatine (Cr) signal amplitude as a denominator. Both quantification methods are established as reliable indicators of a given concentration of metabolite (26). A large difference was observed when the absolute quantities of the 1.28-ppm biomarker were compared between the hippocampal and cortical spectra; this was paralleled by the ratiometric quantification, which confirmed that the hippocampus was highly enriched in the 1.28-ppm biomarker as compared to the cortex (Fig. 3A).

We also transplanted NPCs into the left cortical hemisphere of the adult rat brain and injected an equal volume of saline into the control right hemisphere. ^1H -MRS data were obtained for both hemispheres from voxels of the same size, centered on the injected areas (Fig. 3B). Both Fourier transform (inset) and SVD-based signal processing (colored peaks) clearly detected the 1.28-ppm biomarker in the spectra of the experimental site containing NPCs (Fig. 3B). Both the direct quantification and the ratiometric analysis demonstrated that the signal in the hemisphere with the injected NPCs was more than 35 times greater than that in the corresponding region of the control cortical hemisphere (Fig. 3B).

Furthermore, to detect changes in the density of endogenous NPCs in vivo, we treated adult rats with ECS. Five days after the treatment, we injected BrdU to label dividing cells and analyzed the ECS-treated and sham-operated control animals the next day. Quantification of

the 1.28-ppm:Cr signal amplitude ratios in the hippocampus showed a significant increase of the 1.28-ppm biomarker in ECS-treated rats as compared to sham-operated controls (Fig. 3C). To validate the spectroscopic findings, we quantified the number of BrdU-immunoreactive cells in the hippocampus of the same animals (Fig. 3D). A significant increase in the number of BrdU-immunoreactive cells in ECS-treated rats as compared to sham-operated controls demonstrated that, as expected, ECS increased NPC proliferation. Moreover, in the ECS-treated animals, we found a correlation between the number of BrdU-immunoreactive cells and the 1.28-ppm:Cr signal amplitude ratio in the hippocampus of the same animal (Fig. 3E). Together, these data indicate that ^1H -MRS can be used to detect and measure changes in the density of endogenous NPCs in vivo.

We then proceeded with the identification of endogenous NPCs in the human brain. Brain ^1H -MRS was performed on healthy adults, using a 3-T MRI scanner and SVD-based signal processing (Fig. 4A). An experimental voxel was placed along the length of the hippocampus, while a control voxel of the same volume included gray and white matter of the ipsilateral parietal cortex (Fig. 4A). The Fourier transform did not reveal the 1.28-ppm biomarker (inset) in any of the voxels (Fig. 4A). However, the SVD-based analysis (colored peaks) clearly detected the 1.28-ppm biomarker in the hippocampal spectra, indicating that this methodology can be used to identify endogenous NPCs in the human brain (Fig. 4A). For each person, we found a major difference between the hippocampus and the cortex when using either absolute or ratiometric quantification of the 1.28-ppm biomarker, indicating that both can be applied to indirectly measure NPC density in the human hippocampus. No difference in the level of the 1.28-ppm biomarker was observed when the left and right hippocampi were compared (Fig. 4A). Further-more, when we imaged the left hippocampus of the same people after a 3-month period during which there was no major change in their daily routine, no difference was observed in the 1.28-ppm biomarker (Fig. 4B). Finally, we analyzed the age-related changes in the 1.28-ppm biomarker during human development by imaging people of varying ages: preadolescents, adolescents, and adults. Quantification of the 1.28-ppm biomarker revealed a decrease in the 1.28-ppm signal amplitude (Fig. 4C), which is compatible with data demonstrating age-related decrease in neurogenesis in animals (27).

In our work, we identified a spectroscopic biomarker of NPCs, developed a methodology to detect this biomarker in the live brain, and demonstrated the use of the biomarker for identifying NPCs in the live human brain. The NPC biomarker could be readily detected in vitro with ^1H -NMR, but its detection at low concentrations in the live brain with ^1H -MRS required the development of more refined methodology. Our SVD-based signal processing proved to be superior to the traditionally used Fourier transform and can now be applied in a variety of imaging settings where low levels of a particular metabolite preclude its reliable detection in vivo.

Our results suggest that the NPC biomarker, represented by a 1.28-ppm spectral peak, is a complex mixture of saturated and/or monounsaturated fatty acids and related compounds. The functional relevance of these molecules for the control of proliferation and differentiation of NPCs remains to be elucidated.

Finally, our data on humans provide in vivo imaging evidence for NPCs in the human hippocampus. These findings support the numerous data demonstrating continuous neurogenesis in the dentate gyrus (1, 2, 28). We also demonstrated that in humans the presence of the NPC biomarker in the hippocampus dramatically decreases with age. Although a decrease in neurogenesis has been reported in aging mammals, these are the first data from the living human brain that indicate a decrease in NPCs during brain development from childhood to adulthood. More generally, this biomarker can be applied to track and analyze endogenous or transplanted NPCs, to monitor neurogenesis in a wide range of human neurological and psychiatric disorders, and to evaluate the efficiency of therapeutic interventions.

Supplementary Material

Refer to Web version on PubMed Central for supplementary material.

Acknowledgments

We thank M. Ziliox and K. DeCock for expert technical assistance with ¹H-NMR spectroscopy; B. Forester for mMRI assistance; H. Cognato for OPC cultures; S. Tsirka for microglial cultures; J.-H. Park for advice on ECS; and A. Sierra, J. M. Encinas, J. S. Trimmer, P. Stavropoulos, and J. Banerji for helpful discussions. This work was supported by the National Institute of Neurological Disorders and Stroke (NINDS) (grants R21NS05875-1 and 5K08 NS044276); U.S. Army Medical Research (grant DAMD170110754) (M.M.-S.); the National Institute of Diabetes and Digestive and Kidney Diseases (grant T32DK07521-16) (L.N.M.); NINDS grant R01-NS32764; NARSAD; the Seraph Foundation; the Hartman Foundation; the Hope for Depression Foundation; the Hazan Foundation (G.E.); the U.S. Department of Energy (grant FWP MO-065) (H.B.); NSF (grant CCF-0515246); and the Office of Naval Research (grant N00014-06-1-0012) (P.D.).

References and Notes

1. Lie DC, Song H, Colamarino SA, Ming GL, Gage FH. *Annu. Rev. Pharmacol. Toxicol.* 2004; 44:399. [PubMed: 14744252]
2. Ming GL, Song H. *Annu. Rev. Neurosci.* 2005; 28:223. [PubMed: 16022595]
3. Curtis MA, et al. *Science.* 2007; 315:1243. [PubMed: 17303719]
4. Goldman SA, Windrem MS. *Philos. Trans. R. Soc. London Ser. B.* 2006; 361:1463. [PubMed: 16939969]
5. Cicchetti F, et al. *Contrast Media Mol. Imaging.* 2007; 2:130. [PubMed: 17583908]
6. Chin BB, et al. *Nucl. Med. Commun.* 2003; 24:1149. [PubMed: 14569169]
7. Arbab AS, Liu W, Frank JA. *Expert Rev. Med. Devices.* 2006; 3:427. [PubMed: 16866640]
8. Viant MR. *Methods Mol. Biol.* 2007; 358:229. [PubMed: 17035689]
9. Ross B, Bluml S. *Anat. Rec.* 2001; 265:54. (New Anat). [PubMed: 11323770]
10. Shinno H, et al. *J. Neurol. Sci.* 2007; 260:132. [PubMed: 17540407]
11. Stengel A, et al. *Magn. Reson. Med.* 2004; 52:228. [PubMed: 15282804]
12. Narayana PA. *J. Neuroimaging.* 2005; 15:46S. [PubMed: 16385018]
13. Mignone JL, Kukekov V, Chiang AS, Steindler D, Enikolopov G. *J. Comp. Neurol.* 2004; 469:311. [PubMed: 14730584]
14. Mignone JL, et al. *Cell Cycle.* 2007; 6:2161. [PubMed: 17873521]
15. Bhardwaj RD. *Proc. Natl. Acad. Sci. U.S.A.* 2006; 103:12564. [PubMed: 16901981]
16. van Praag H, Kempermann G, Gage FH. *Nat. Neurosci.* 1999; 2:266. [PubMed: 10195220]
17. Kempermann G, Kuhn HG, Gage FH. *Nature.* 1997; 386:493. [PubMed: 9087407]
18. Encinas JM, Vaahtokari A, Enikolopov G. *Proc. Natl. Acad. Sci. U.S.A.* 2006; 103:8233. [PubMed: 16702546]

19. Warner-Schmidt JL, Duman RS. *Hippocampus*. 2006; 16:239. [PubMed: 16425236]
20. Madsen TM, et al. *Biol. Psychiatry*. 2000; 47:1043. [PubMed: 10862803]
21. Perera TD, et al. *J. Neurosci*. 2007; 27:4894. [PubMed: 17475797]
22. Sparling ML, Zidovetzki R, Muller L, Chan SI. *Anal. Biochem*. 1989; 178:67. [PubMed: 2729581]
23. Barkhuijsen H, de Beer R, van Ormondt D. *J. Magn. Reson*. 1987; 73:553.
24. Cavassila S, et al. *J. Magn. Reson. Anal*. 1997; 3:87.
25. Stoica P, Sandgren N, Selen Y, Vanhamme L, Van Huffel S. *J. Magn. Reson*. 2003; 165:80. [PubMed: 14568518]
26. Dieterle F, Ross A, Schlotterbeck G, Senn H. *Anal. Chem*. 2006; 78:4281. [PubMed: 16808434]
27. Kuhn HG, Dickinson-Anson H, Gage FH. *J. Neurosci*. 1996; 16:2027. [PubMed: 8604047]
28. Eriksson PS, et al. *Nat. Med*. 1998; 4:1313. [PubMed: 9809557]

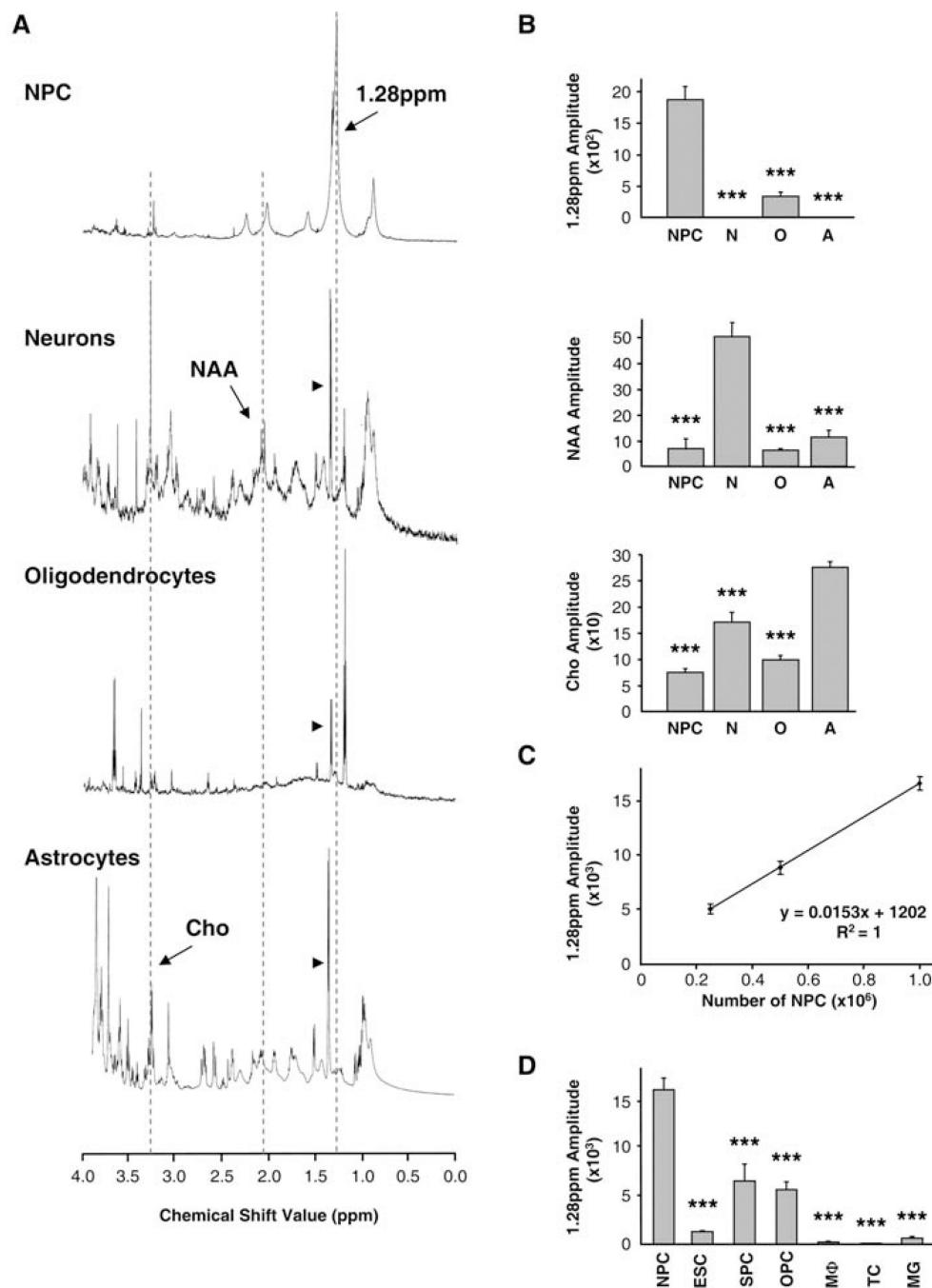
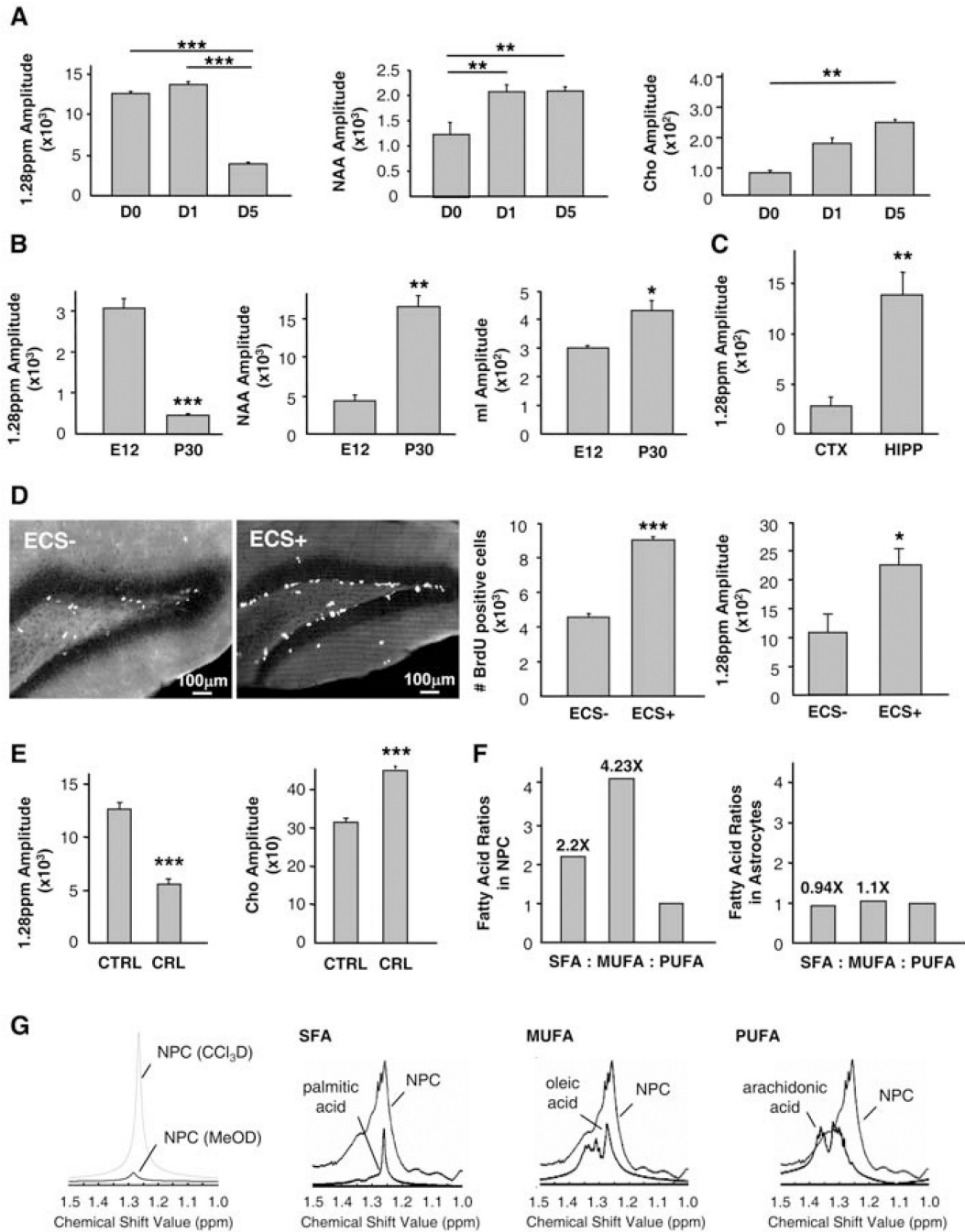


Fig. 1. The 1.28-ppm biomarker identifies NPCs. **(A)** Spectral profiles of cultured neural cell types: NPCs, neurons, oligodendrocytes, and astrocytes. Dotted lines outline the 1.28-ppm NPC peak, NAA (2.02 ppm), and Cho (3.23 ppm). Arrowheads denote lactate doublets (1.33 ppm). Spectra are not of equal scale. **(B)** Bar graphs show quantification of the 1.28-ppm biomarker (top), NAA (middle), and Cho (bottom) (2.5×10^5 cells each, $n = 3$ experiments per group, done in triplicate samples per experiment). N, neurons, O, oligodendrocytes, A, astrocytes. **(C)** Quantification of the 1.28-ppm biomarker shows correlation of the number

of NPCs and the 1.28-ppm signal amplitude ($n = 3$ experiments per data point, done in triplicate samples per experiment). **(D)** Quantification of the 1.28-ppm biomarker in proliferating cells: NPCs, ESCs, SPCs, OPCs, macrophages ($M\Phi$), T lymphocytes (TC), and microglia (MG) (1×10^6 each, $n = 3$ experiments per group, done in triplicate samples per experiment). For all figures, quantification was done with the SVD-based method; bar graphs represent mean \pm SEM; *, $P < 0.05$; **, $P < 0.01$; ***, $P < 0.001$. Detailed statistics are provided in the supporting online material.

**Fig. 2.**

Analysis of the specificity and molecular composition of the NPC biomarker using ^1H -NMR. (A) Quantification of NPC, neuronal (NAA), and glial (Cho) biomarkers during in vitro differentiation, at 0, 1, and 5 days (D) after neurosphere plating (1×10^6 cells per time point, $n = 3$ experiments per time point, done in triplicate samples per experiment). (B) Quantification of NPC, neuronal (NAA), and glial (mI) biomarkers in whole-brain homogenates at E12 and P30 (1×10^6 cells per time point, $n = 3$ experiments per time point, done in triplicate samples per experiment). (C) Quantification of the NPC biomarker in the

dissociated adult mouse cortex (CTX) and hippocampus (HIP) (1×10^6 cells per group, $n = 3$ experiments per group, done in triplicate samples per experiment). **(D)** ECS increases both the number of BrdU-immunoreactive cells ($n = 3$ experiments; $P < 0.01$) and the 1.28-ppm biomarker ($n = 3$ experiments; $P < 0.05$) in the mouse hippocampus. **(E)** The 1.28-ppm biomarker diminishes while Cho increases upon blockade of fatty acid synthesis with cerulenin (CRL) ($n = 3$ experiments per group, done in triplicate samples per experiment, $P < 0.001$). **(F)** SFAs and MUFAs are more abundant in NPCs than in astrocytes ($n = 1$). **(G)** The 1.28-ppm biomarker belongs to a chloroform (CCl_3D) and not methanol (MeOD) fraction. It overlaps with SFAs and MUFAs rather than PUFAs.

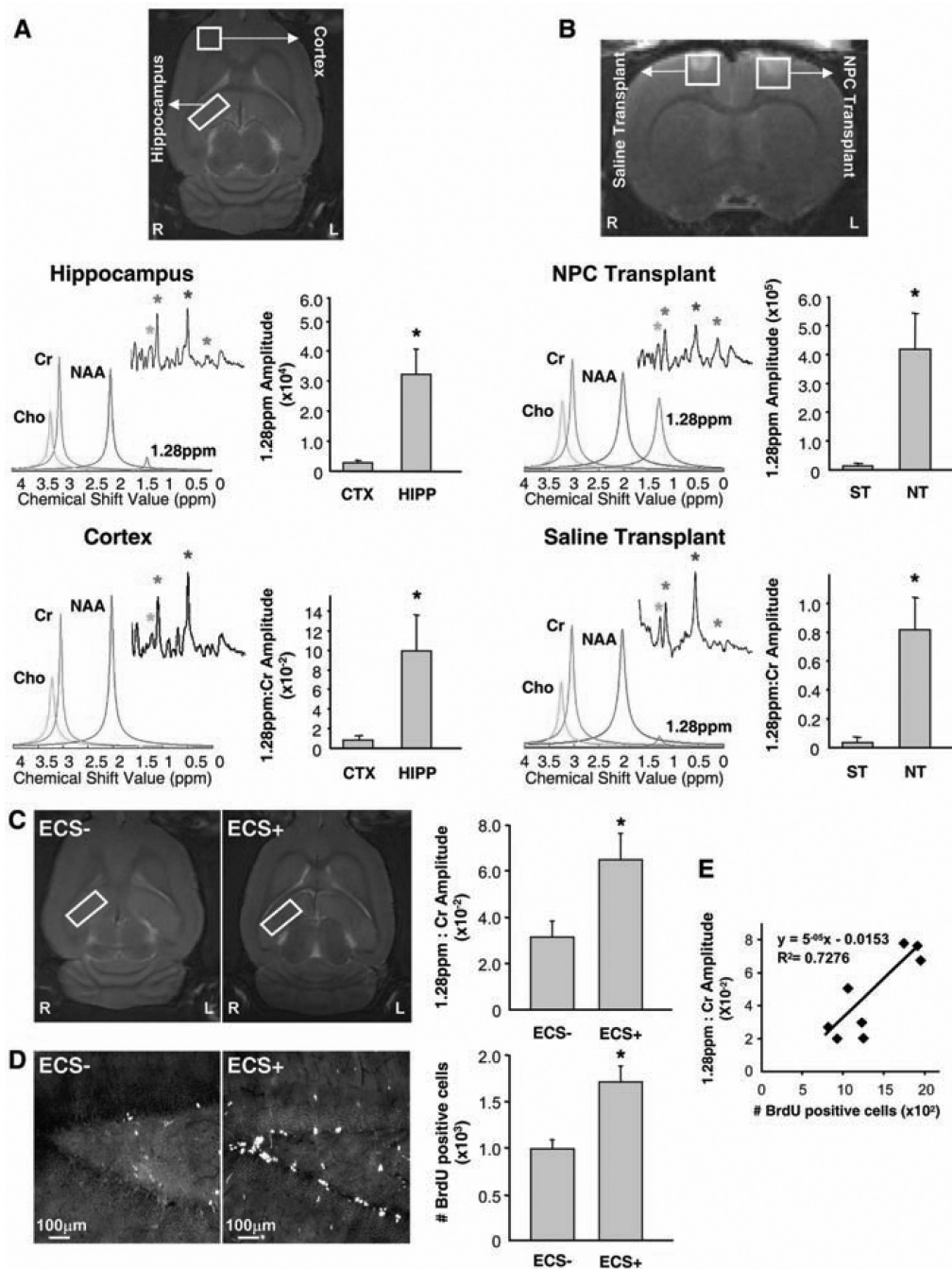


Fig. 3. Identification of NPCs in the rat brain in vivo, using mMRI spectroscopy. **(A)** Imaging of endogenous NPCs. Voxels are placed along the hippocampus (HIPP) and in the cortex (CTX). In the hippocampus, the 1.28-ppm biomarker (red) is evident when SVD-based signal processing is performed (colored peaks) but not when Fourier transform is done (insets). In the cortex, the 1.28-ppm biomarker is not detected by either data analysis. Colored asterisks and peaks correlate. Bar graphs show absolute (top) and relative (bottom) quantification of the 1.28-ppm biomarker ($n = 4$ experiments, $P < 0.05$). **(B)** Imaging of

transplanted NPCs. Voxels are placed in the area of NPC transplant (NT; 5×10^6 NPCs in 5 ml of saline) and saline injection (ST; 5 μ l). In the NT site, the 1.28-ppm biomarker (red) is observed with both Fourier transform and SVD-based signal processing. In the ST site, no significant 1.28-ppm signal is observed. Bar graphs show absolute (top) and relative (bottom) quantification of the 1.28-ppm biomarker ($n = 5$ experiments; $P < 0.05$). (C and D) Imaging of endogenous NPCs after ECS. Voxels are placed along the hippocampus in control (ECS-) and ECS-treated (ECS+) adult rats (C). Quantification of the 1.28-ppm biomarker [(C) $n = 4$ experiments, $P < 0.05$] and the number of BrdU-immunoreactive cells in the dentate gyrus of the same animal [(D) $n = 4$ experiments, $P < 0.01$] indicates linear correlation (E).

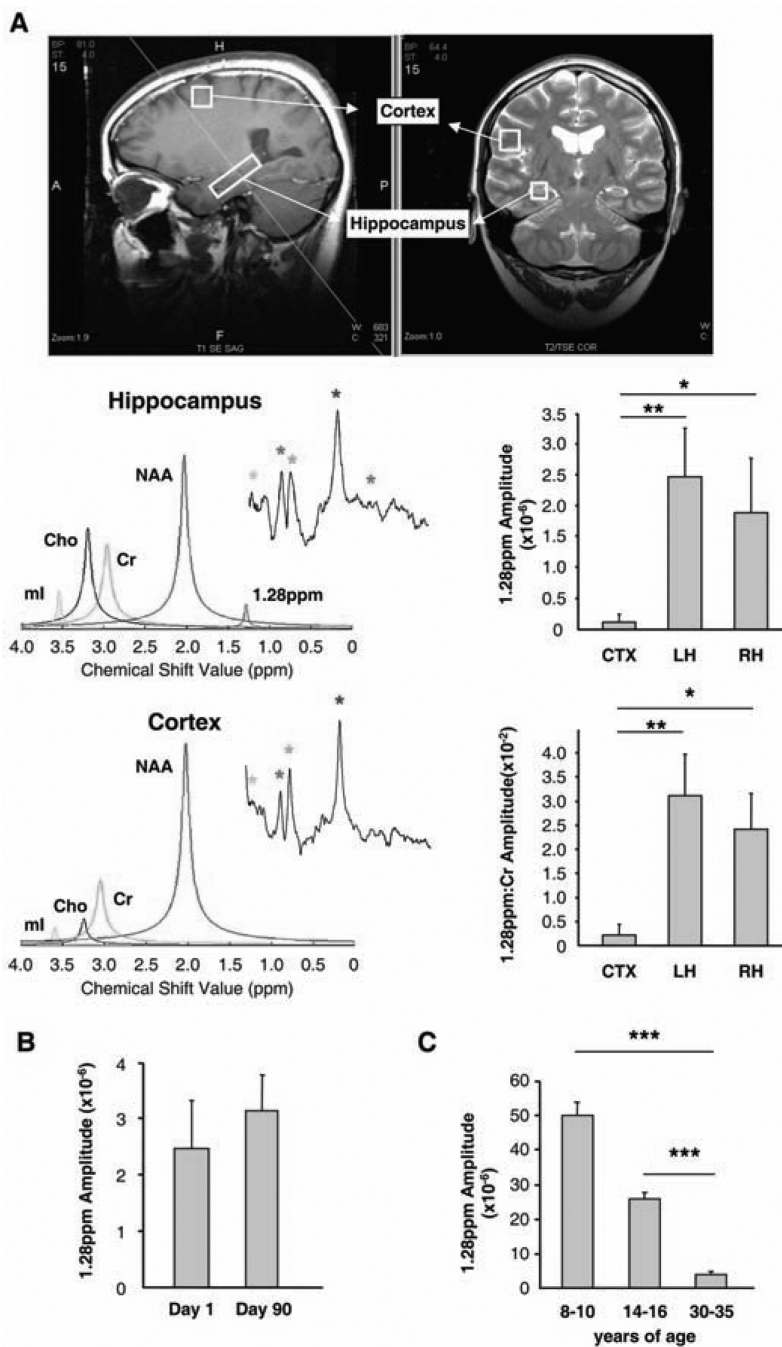


Fig. 4. Identification of NPCs in the human hippocampus in vivo, using ¹H-MRS. (A) Voxels are placed along the hippocampus and in the cortex. In the hippocampus, the 1.28-ppm biomarker (red) is evident when SVD-based signal processing is performed but not when Fourier transform is done. In the cortex, the 1.28-ppm biomarker is not detected by either data analysis. Colored asterisks and colored peaks correlate. Bar graphs show absolute (top) and relative (bottom) quantification of the 1.28-ppm biomarker (CTX, cortex; LH, left hippocampus; RH, right hippocampus; *n* = 5people; *P* < 0.01 and *P* < 0.05, respectively).

(B) Quantification of the 1.28-ppm biomarker in the adult human hippocampus over time ($n = 4$ people, $P = 0.747$). The same people were imaged 90 days apart. **(C)** Quantification of the 1.28-ppm biomarker in the human hippocampus during development in preadolescent, adolescent, and adult age groups ($n = 3$ people per group; $P < 0.001$).